Nanocolumnar coatings with selective behavior towards osteoblast and *Staphylococcus aureus* proliferation

Isabel Izquierdo-Barba[1,2], *José Miguel García-Martín*[3], *Rafael Álvarez*[4], *Alberto Palmero*[4], *Jaime Esteban*[5], *Concepción Pérez-Jorge*[5], *Daniel Arcos*[1,2,*], *María Vallet-Regí*[1,2],*

1. Departamento de Química Inorgánica y Bioinorgánica. Facultad de Farmacia, Universidad Complutense de Madrid. Instituto de Investigación Sanitaria Hospital 12 de Octubre i+12. Plaza Ramón y Cajal s/n, 28040 Madrid, Spain.

2. CIBER de Bioingeniería, Biomateriales y Nanomedicina (CIBER-BBN), Spain

E-mail: vallet@ucm.es; arcosd@ucm.es

3. IMM-Instituto de Microelectrónica de Madrid (CNM-CSIC), Isaac Newton 8, PTM, E-28760 Tres Cantos, Madrid, Spain

4. Instituto de Ciencia de Materiales de Sevilla (CSIC-Universidad de Sevilla). Americo Vespucio 49, 41092 Seville, Spain

5. Department of Clinical Microbiology. IIS-Fundación Jiménez Díaz, Universidad Autónoma de Madrid, Spain

*Corresponding authors: Vallet@ucm.es, arcosd@ucm.es Tel: +34 913941843

Abstract

Bacterial colonization and biofilm formation on orthopedic implants is one of the worst scenarios in orthopedic surgery, in terms of both patient prognosis and healthcare costs. Tailoring their surfaces at the nanoscale to actively promote bone bonding, while avoiding bacterial colonization represents an interesting challenge to reach better clinical outcomes. Herein, a Ti6Al4V alloy of medical grade has been coated with Ti nanostructures employing the glancing angle deposition technique by magnetron sputtering. The resulting surfaces have a high density of nanocolumnar structures, which exhibit strongly impaired bacterial adhesion inhibiting the biofilm formation while the osteoblast exhibit good cell response with similar behavior than the initial substrates. These results are discussed on the basis of a "lotus leaf effect" induced by the surface nanostructures and the different size and biological characteristics of osteoblasts and *S. aureus*.

Keywords: Titanium nanocolumns, magnetron sputtering, biocompatibility, antibacterial effects, biofilm

1. Introduction

Orthopedic prosthetic implants save and/or improve the quality of life of millions of patients every year [1]. On the basis of their excellent biocompatibility and good mechanical properties, some metallic alloys are generally employed to manufacture devices such as join prostheses, fracture fixation elements, external fixators, etc. One of the most serious complications of prosthetic devices, in terms of morbidity, mortality and medical costs is the incidence of infection [2]. Even though its occurrence has significantly diminished thanks to clinical staff training, control of sterility and protocols of antibiotic prophylaxis, a marginal risk as low as 0.5 – 5 % (only for total join arthroplasty) implies thousands of infected prostheses and other orthopedic devices every year [3,4], an issue of increasing relevance due to the larger amount of patients that undergo prosthetic joint surgery at present.

Most of the infections in metallic orthopedic implants are caused by staphylococci. [5] Among them, both, *Staphylococcus aureus* and *Staphylococcus epidermidis*, represent the two most active species on metallic biomaterials, e.g., stainless steel, CrCo, Ti and Ti alloys. [6,7] In this sense, it is well-known that once bacteria attach to the implant surface, a biofilm is formed that provides antibiotic resistance, becoming the main pathogenic factor for chronic infections.[8-10] In fact, one of the milestones in this research field consists in the development of implant surfaces that diminish the bacterial adherence and the formation of the biofilm. Campoccia *et al* [11] have reviewed different technologies aimed at developing infection resistant surfaces, and other reports indicate that the use of nanostructured surfaces with inhibited bacterial adhesion could represent a challenging alternative to antibiotics.[12-14] Besides, several research groups have demonstrated that nanostructured biomaterials may improve the osteoblasts response [15-17] and Anselme *et al* have highlighted [18] that the development of surfaces with simultaneous opposite responses towards osteoblast or bacteria proliferation may represent a relevant achievement in orthopedic implantology. In the literature, there are very few studies that analyze surfaces that fulfill both conditions, and

none of them on materials employed in the manufacture of orthopedic devices, [19,20] with the exception of reference [21], that focuses on commercially pure Ti for dental applications. The idea of tailoring surfaces with customized and selective responses towards each specific cell was also suggested by Decuzzi and Ferrari.[22] They proposed a mathematical model that indicated the key role of the surface nanotopography in the stimulation of osteoblast-like cells while reducing bacterial adhesion and proliferation. In a recent publication, the antibacterial activity of titanium nanostructured surfaces fabricated onto silicon wafers has been reported, [23] showing that these were active against gram-negative *E. coli* but inefficient against gram-positive *S. aureus*. As stated by the authors, these coatings "*are not meaningful in the orthopedic field, in which a very large proportion of all implant-related infections are caused by Staphylococci*". Overall, and regarding the state of the art in the area of orthopedic implants, a significant advance in the development of infection resistant coating (prior to an *in vivo* analysis) should comprise the following features: (i) It must be tested onto substrates made of medical grade biomaterials, (ii) it should not diminish the human osteoblasts adhesion and proliferation, (iii) it should exhibit antibacterial behavior against the most pathogenic bacteria in orthopedic related infections. In particular, it should avoid the formation of the biofilm and (iv) it should present antibacterial properties not only respect to collection strains but also to clinical ones, *i.e.* those isolated from patients with infection, since their behavior can be different.

Herein, we report the preparation of nanocolumnar patterned surfaces made of titanium by means of the so-called glancing angle deposition technique by magnetron sputtering (MS-GLAD). The MS-GLAD is a powerful technique to produce nanostructured coatings in large areas and with a large variety of morphologies. [24,25] It is based on exploiting atomic shadowing effects during physical vapor deposition in high vacuum conditions. MS-GLAD is widely employed in microelectronics as well as in other fields of nanotechnology, both in research and in industrial mass-production facilities due to the high

growth rate of the obtained coatings, the possibility to work on large areas at room temperature and its versatility to fine-tune atomistic self-assembly processes on surfaces [26]. In recent works we have studied in detail MS-GLAD [24,27], where we have demonstrated that the main processes responsible for the formation of the nanostructures are the atomic self-shadowing mechanism at the surface and the collisional processes of the sputtered atoms in the plasma phase, mediated by the tilt angle of the substrate and the value of the argon background pressure.

Our final aim is to prepare nanocolumnar coatings made of Ti on typical orthopedic device material (Ti6Al4V) that preserve the biocompatibility towards osteoblast while the *S. aureus* adherence dramatically fall. Furthermore, the formation of a biofilm of such bacteria should be inhibited, which is a key factor to prevent the infection of the prosthesis. To our knowledge, this is the first experimental demonstration that a nanostructured coating onto medical grade Ti6Al4V exhibits compatibility towards osteoblasts adhesion and proliferation whilst reducing *S. aureus* adhesion, proliferation and biofilm formation.

2. Materials and Methods

2.1. Fabrication of the nanostructured coating

Medical grade Ti6Al4V substrates of 12 mm diameter and 2 mm of thickness (Biomet Spain Orthopedic S.L.) were mechanically polished to mirror by a sequence of diamond pastes until colloidal silica (0.25 μm) finishing. Such disks were used as substrates to be coated with titanium nanocolumns by MS-GLAD. For this purpose, the Ti vapor flux was produced by the magnetron sputtering technique employing a 5 cm diameter Ti target and argon as the sputter gas. The substrates were placed at 22 cm from the target and tilted 80° with respect to its normal. The base pressure of the chamber was in the mid 10^{-9} mbar range, whereas the deposition was carried out at a pressure of 1.5×10^{-3} mbar and employing a DC electromagnetic power generator set at 300 W. Under these conditions, the deposition rate was 0.3 Å/s, the substrate temperature being always below 330ºK during the growth of the

nanostructured coating. Only one surface of the disks was coated. The coated Ti6Al4V substrates will be referred from now forth as Nano-Ti6Al4V. For comparison purposes, uncoated substrates of the same medical grade Ti6Al4V were also included in all the experiments.

2.2. Material surface characterization

Powder X-ray diffraction (XRD) patterns were recorded in a Philips Model X'Pert diffractometer using Cu Kα radiation (wavelength of 1.5406 Å). They were collected in the 2θ range of 20º - 80º, with a step size of 0.02º and a counting time of 0.5 s per step. In order to collect information preferentially from the disks surface, the grazing incidence diffraction (GID) method was applied using a grazing angle ω of 0.5º. In this method, the stationary incident beam makes a very small angle with the sample surface (typically 0.3°to 3°), which increases the path length of the X-ray beam through the coating. This helps to increase the diffracted intensity, while at the same time, reduces the diffracted intensity from the substrate and the conventional phase identification analysis can be run. Fourier transform infrared (FT-IR) spectra were collected in a Thermo Nicolet Nexus spectrometer (Thermo Scientific, USA) equipped with a Goldengate attenuated total reflectance (ATR) device. Contact angles were measured to estimate the wettability of the samples. The experiments were performed by the sessile drop method at 25 ºC on a CAM 200 KSV contact angle goniometer. Pictures of the drops were taken every 1 s. The software delivered by the instrument manufacturer calculated the contact angles on the basis of a numerical solution of the full Young-Laplace equation.

Atomic force microscopy (AFM) measurements were performed using a Dimension Icon microscope from Bruker operating in non-contact mode. The probes were model TESP-SS, with resonant frequency around 300 kHz, spring constant about 40 N/m, and a sharp spike tip at the end with 2 nm nominal radius. The root mean square (RMS) roughness was measured in a 2x2 μm^2 area.

2.3. Osteoblasts in vitro cell cultures

Before osteoblast cells *in vitro* assays, all samples were sterilized by dried heat at 150 ºC for 12 h. Due to the presence of a TiO_2 phase on the surface of the samples when exposed to air, we have intentionally avoided the use of ultraviolet light during the whole analysis of the samples to avoid any photoactive response of the layers.[28] Human osteoblast-like (HOS) cell line obtained through the European Collection of Cell Cultures denoted HOS (ECACC, no. 87070202) was used. Cells were cultured in a complete medium consisting of Dulbecco's modified Eagle medium (DMEM) (Sigma Chemical Co., St. Louis, USA) supplemented with 2 mM L-glutamine (Gibco, Invitrogen Corporation, USA), 100 U mL^{-1} penicillin (Life technologies limited, Scotland), 100 g mL^{-1} streptomycin (Life technologies limited, Scotland), and 10% fetal bovine serum (FBS) (Gibco, Invitrogen Corporation, USA) at 37ºC in a humidified atmosphere of 95% air and 5% CO_2. Osteoblast-like cells were routinely subcultured by trypsinization. Then, HOS cells were seeded onto the different samples previously placed into 24-well culture plates at a seeding density of 2.5x 10^5 cells per mL in the complete medium under a CO_2 (5%) atmosphere at 37ºC for different time periods for each in vitro assays.

Cell adhesion assay. For cell attachment experiments, samples were incubated under standard culture conditions during 90 min. After that, the samples were washed three times in phosphate buffered solution (PBS). After that, the attached cells to the different surfaces were unattached by trypsin treatment during 10 min. The cells were centrifuged, resuspended in PBS and counted in Neubauer chamber. Data are expressed as means ± standard deviations of three experiments. Tissue culture plastic was used as control.

Cell-spreading assays. The attached cells were rinsed three times in PBS and fixed with 2.5% glutaraldehyde (50% wt. Sigma-Aldrich, USA) in PBS during 45 min. Sample dehydration was performed by slow water replacement, using a series of ethanol solutions (30%, 50%, 70%, 90%) for 30 min with a final dehydration in absolute ethanol for 60 min, allowing

samples to dry at room temperature and under vacuum. Thereafter, the samples were mounted on stubs and gold coated in vacuum using a sputter coater (Balzers SCD 004, Liechtenstein) and visualized by SEM using a field emission JEOL JSM-6335F microscope (Tokyo, Japan) at an acceleration voltage of 10 kV.

Cell mitochondrial activity. Cell proliferation was determined in terms of cell mitochondrial activity. For this purpose, HOS cells were seeded onto the material surface in 24-well plates at a density of 10^5 cells per mL in the complete medium and incubated under standard conditions. Cell proliferation determinations were performed using the (3-[4,5-dimethylthiazol-2-yl]-2,5-diphenyltetrazolium bromide) (Sigma-Aldrich, USA) MTT assay at different time periods after seeding. Tissue culture plastic was used as control.

Statics of biocompatibility assays. Data are expressed as means +/- standard deviations of three experiments. Statistical analysis was performed using the Statistical Package for the Social Sciences (SPSS) version 11.5 software. Statistical comparisons were made by analysis of variance (ANOVA). The Scheffe's test was used for post hoc evaluations of differences among groups. In all statistical evaluations, $p < 0.05$ was considered as statistically significant.

2.4. Bacteria in vitro tests

Bacterial adhesion test. Prior to the bacteria adhesion tests Ti6Al4V and nano-Ti6Al4V samples were sterilized by dried heat at 150 ºC for 12 h. Bacterial adhesion studies have been performed on different Ti6Al4V surfaces using a *S. aureus* 15981 laboratory strain and six clinical strains identified as P1, P2, P4, P18, P61T3, and P95. The clinical strains were isolated by a sonication procedure from patients who have had an orthopedic implant-related infection. For the adhesion experiments, bacteria were inoculated in tryptic soy broth (TSB; BioMerieux, Marcy L'Etoile, France) and incubated overnight at 37ºC with 5% CO_2. After culture, bacteria were centrifuged for 10 min at 3500g at 22ºC. Supernatant was then discarded, and the pellet was washed three times with sterile phosphate-buffered saline (PBS;

Sigma-Aldrich Life Science). Bacteria were then suspended and diluted in PBS to obtain a 10^8 CFU/mL concentration; the bacterial concentration was determinate by spectrophotometry using a visible spectrophotometer (Genesys 20, Thermo Scientific). Different specimens of Ti6Al4V were inoculated with the bacterial solutions during 90 min to allow adhesion in a static model. After that, the samples were washed three times with PBS to remove unattached bacteria. Finally, they were stained for 15 min with Live/Dead ® Bacterial Viability Kit (BacklightTM). Staining is performed with a mixture of dyes, SYTO 9 (live bacteria/green) and propidium iodide (dead bacteria/red). SYTO 9 fluorescence was excited at 480/500 nm and the emitted fluorescence measured at 500 nm and propidium iodide fluorescence was excited at 490/635 nm and the emitted fluorescence measured at 618 nm.[28] Eight photographs (40x magnification) by ultraviolet (UV) microscope for each sample were made. The surface area covered with adhered bacteria was calculated using ImageJ software (National Institute of Health, Bethesda, MD). The experiments were performed in triplicate for each strain.

Confocal microscopy. The confocal microscopy studies were carried out with a Biorad MC1025 confocal laser scanning microscope (CLSM). The different specimens were stained with BacklightTM dye as previously described.

Biofilm formation test. Both surfaces were suspended in bacteria solution of *S. aureus* strain (10^8 bacteria/mL) and incubated during 24 hours in a 66% tryptic soy broth (TSB) plus 0.2% glucose medium to promotes robust biofilm formation (20 g/liter of Difco Bacto tryptic soy broth, Becton Dickinson, Sparks, MD). After 24 hours, both surfaces were washed 3 times with sterile PBS and stained with 3 μl of Syto-9/propidium iodide mixture incubated during 15 min and posterior washed with PBS.

To determine most specifically the biofilm formation we used calcofluor, a fluorescent dye that has been used to stain the extracellular matrix of biofilms. In this case, 1 ml of calcofluor solution (5mg/ml) was inoculated after Syto-9/propidium iodide mixture addition and was

incubated during 15 min at room temperature. Biofilm formation was examined using a LEICA SP2 Confocal Laser Scanning Microscope. Confocal 3D image reconstruction were carrie out from 45 Z stacks in an Olympus FV1200 confocal microscope.

Statistics for bacterial studies. The results obtained were presented comparing the mean percentage of covered biomaterial surface for untreated and sputtered specimens, respectively by using EPI-INFO software version 3.5.1 (CDC, Atlanta, GA). To carry out the statistical study, nonparametric tests were performed.

3. Results and Discussion

SEM micrographs evidence the different surface features between Ti6Al4V (Fig. 1.a) and Nano-Ti6Al4V (Figure 1b). After MS-GLAD, the Nano-Ti6Al4V substrate appears fully coated, with patterns in the nanoscale. The nanotopography of the analyzed coatings consists of almost vertically aligned nanocolumns with lengths between 250 and 350 nm, diameters between 40 and 60 nm, and separated (from center to center) between 100 and 200 nm (Figure 1c and 1d). In this way the coating fully covers the Ti6Al4V material with numerous nanofeatures per unit area. It has been described that this kind of dense and highly packed nanotopographies, together with the separation between nanofeatures can lead to a significant decrease of wettability due to a lotus leaf effect on the material surface. [29-31]. In order to estimate the wettability of the samples, contact angles measurements were carried out. Despite the fact that the measured contact angle does not classify Nano-Ti6Al4V as superhydrophobic, the wettability of the Ti6Al4V substrate dramatically decreases after being coated with the Ti nanocolumns (Fig. 1e and 1f). The contact angle for the initial Ti6Al4V substrate is 56º, whilst that of Nano-Ti6Al4V is 102º.

Fig. 2 shows the grazing incidence X-ray diffraction (GI-XRD) patterns for Ti6Al4V and Nano-Ti6Al4V. The maxima for Ti6Al4V alloy can be assigned to the hexagonal α-Ti phase (the major phase in Ti6Al4V alloys) with space group P63/mmc. However, the pattern corresponding to Nano-Ti6Al4V also shows diffraction maxima that can be assigned to TiO_2

rutile phase with space group P42/mm. These results indicate the presence of crystalline TiO_2 rutile onto the Nano-Ti6Al4V samples. This oxide layer is formed when exposing the material to the atmosphere, which induced the oxidation of the first atomic monolayers, as evidenced by the TiO_2 maxima found in the XRD pattern.

Attenuated total reflectance- Fourier transform infrared (ATR-FTIR) spectroscopy are shown in Fig. 3. FTIR spectra obtained by means of ATR method mainly collect information from the samples surfaces. The spectra collected for Ti6Al4V shows absorption bands between 2550 and 3550 cm^{-1}. This wide interval of vibrations corresponds to the stretching vibration of O-H bonds in different situations at the alloy surface, i.e. isolated Ti-OH groups, undergoing intermolecular forces, polymeric units, adsorbed water, etc.[32] The bands at 1200 cm^{-1} and 1083 cm^{-1} correspond to the phonon mode vibration of Al_2O_3 [33] (commonly present in Ti6Al4V alloys). Finally, the band at 916 cm^{-1} can be assigned to the Ti-O-Ti vibrational mode, thus indicating the presence of a thin titanium oxide layer at the substrate, commonly present in these alloys as consequence of dry passivation.

The FTIR spectrum for Nano-Ti6Al4V shows similar absorption bands. However there are significant differences in the wideness of the frequency interval. For instance, the band assigned to the O-H stretching vibration is centered in a lower frequency interval between 2900 and 2600 cm^{-1}. This fact indicates that hydroxyls groups with lower O-H energy bond predominate at the surface of Nano-Ti6Al4V, which is indicative of electron charge transference due to hydrogen bonding between neighbors hydroxyl groups. The vibrational modes of Ti-O-Ti appear in a wide interval of frequencies from 950 to 500 cm^{-1}, which is indicative of different states for the TiO_2 layer onto Nano-Ti6Al4V surface. The phonon mode vibration of Al_2O_3 does not appear in the FTIR spectra for Nano-Ti6Al4V. FTIR spectra of Nano-Ti6Al4V collected by ATR indicates a more ordered arrangement of Ti-OH groups, where OH groups would be close enough to form hydrogen bonds, as deduced from the prevalence of the stretching O-H signals at lower frequencies. On the contrary, FTIR

spectra obtained for Ti6Al4V point out a more disordered arrangement of the Ti-OH groups. Both, XRD and FTIR results indicate the formation of crystalline rutile over the nanocolumns topography, whereas the TiO_2 layer formed over polished substrates seems to be a non-ordered phase.

Atomic force microscopy (AFM) measurements were performed to characterize the nanotopography of the Ti6Al4V substrates (Fig. 4a) and the Nano-Ti6Al4V samples (Fig. 4b). Ti6Al4V substrates exhibit several scratches due to the mechanical polishing and the root mean square (RMS) roughness of the whole 2x2 μm^2 area is about 3nm. After the growth of the coating by magnetron sputtering, the surface of Nano-Ti6Al4V is homogeneously coated with Ti nanocolumns, as can be clearly seen in Figure 4b. The measured RMS roughness is 57 nm in this case, although this value must be understood as an underestimation, since the AFM tip could not penetrate down to the very bottom of some inter-columnar spaces due to their high aspect ratio.

Once both Ti6Al4V and Nano-Ti6Al4V surfaces were characterized, we proceeded to evaluate the *in vitro* biocompatibility by culturing human osteoblast-like (HOS) cell line on them. The initial (90 minutes) osteoblast adhesion (Fig. 5a) does not show significant differences between the medical grade Ti6Al4V substrate, the Nano-Ti6Al4V sample and the control. Besides, the mitochondrial activities of HOS are almost identical for Ti6Al4V and Nano-Ti6Al4V and do not show significant difference after 3 days of culture (Fig. 5b). The observation of the surfaces by SEM after 1 day of culture (Fig. 5 c-f) confirmed that Nano-Ti6Al4V behaves as good as medical grade Ti6Al4V respect to human osteoblasts. The surfaces appear fully covered by cells, exhibiting a good adhesion, proliferation and extension degree in both cases. Higher magnifications (Fig. 5d and Fig. 5f) show the anchoring elements spread by the cells. In the case of Nano-Ti6Al4V, Fig. 5f shows a detail of a broken cell that allows observing the Ti nanocolumns remaining below the osteoblast layer.

Once the biocompatibility of Nano-Ti6Al4V was assessed, we studied the behavior of the Ti nanocolumns when exposed to *S. aureus*: not only to the collection strain 15981 but also to six clinical strains identified as P1, P2, P4, P18, P61T3, and P95, isolated from different patients [34]. The antibacterial effect of Nano-Ti6Al4V surfaces was observed by means of bacterial adhesion experiments in comparison with those on medical grade Ti6Al4V substrates. Nano-Ti6Al4V exhibits a notably decrease of *S. aureus* adhesion for both collection and clinical strains, albeit an interspecies variability exists (Fig. 6). The adhesion of strain 15981 *S. aureus* observed onto Nano-Ti6Al4V surface shows a significant decrease ($p<0.001$, Kruskal -Wallis test) of around 70% with respect to untreated Ti6Al4V surfaces. Furthermore, for the six clinical strains, which exhibit different initial bacterial adhesion, a significant decrease ($p<0.001$, Kruskal -Wallis test) in the percentage of covered surface is also observed, reducing c.a. 68; 71; 69; 66 and 44% for the P1, P2, P4, P18, P95 and P61T3 strains, respectively.

Concerning biofilm formation, our initial observations by SEM after 24 hours of culture pointed out that *S. aureus* 15981developed an extracellular matrix that coated the Ti6Al4V substrates (Fig. 7). On the contrary, the surface of Nano-Ti6Al4V appeared free of this extracellular matrix. This observation impelled us to carry out appropriated studies for biofilm formation assessment. With this purpose in mind, we have performed confocal microscopy to characterize the sequential biofilm formation after different period times using Syto-9/ propidium iodide dyes which label live and dead bacteria in green and red, respectively (Fig. 8a). In agreement with the previous SEM results, the presence of few and scattered bacteria on the Nano-Ti6Al4V surface is noted as well as the absence of biofilm after 24 hours of incubation. The thickness of biological material attached onto both surfaces was determined by analyzing eight different areas of each piece by confocal microscopy. The measured thickness was 21.8 ± 3.3 μm for the Ti6Al4V substrate ($n =8$; $p<0.001$, Kruskal-Wallis test), whilst the statistical software gave 4.8 ±7.8 μm for Nano-Ti6AlV, an invalid

value that means that there is only scattered bacteria on the surface, i. e. no biofilm is formed in this case. These measurements, together with the confocal microscopy images clearly evidence a compact biofilm layer covering the entire non-modified surface of Ti6Al4V and a scattered bacteria adhesion onto the nanostructured Nano-Ti6Al4V surface.

To further analyze these findings, we decided to carry out additional confocal microscopy experiments employing both Syto-9/ propidium iodide (live bacteria in green, dead ones in red) and calcofluor fluorescent stains (calcofluor dye is widely used to stain the extracellular matrix of biofilms). Fig. 8b shows the confocal 3D images corresponding to biofilm formation after 24 hours of incubation. Non-coated Ti6Al4V substrates clearly evidence the biofilm formation by the blue staining (derived of calcoflouor dye) of typical extracellular matrix that covers the bacteria colonies. On the contrary, the blue staining is absent in Nano-Ti6Al4V as can be observed in fig. 8c.

The selective behavior acquired by the Nano-Ti6AlV biomedical alloy can be explained taking into account the morphology of the sample surface at the nanoscale, the cell characteristics and surface chemistry modifications. In general, the cellular response to topographical features on metallic materials is cell-type dependent [35]. Typical osteoblasts sizes range between 10 and 50 μm, and possess a flexible cell membrane that allow them to adapt to different nanotopographies. Moreover, a necessary condition for them to adhere on a surface is the adsorption of integrins, a mechanism that is diminished on materials with chemical hydrophobic surfaces. Under the light of our results, and the excellent adhesion of osteoblasts onto both Ti6Al4V and Nano-Ti6Al4V, it seems that osteoblast exhibit little sensitivity to the topological features of the studied surfaces. Although a clear conclusion on this issue is far from the scope of this paper, our results suggest that the morphological-induced hydrophobicity of the Nano-Ti6Al4V does not restrain integrins from being absorbed by the surface, allowing the formation of complexes known as focal contacts that attach the osteoblasts to the surface.[18,36,37] After this adhesion, the osteoblasts develop filopodia and

lamellipodia to probe the environment, anchoring and moving, as well as allowing the biointegration of the material. In this regard, some studies in the literature have demonstrated that a corrugated topography with surface nanofeatures (grooves ridges, pits, etc.) separated distances in the order of the micrometer can influence the cell adhesion.[38-41] In our case, the high density of nanocolumns and the very short distance among them (about 100 nm) seems to be undetectable by such large cells as osteoblast, and these nanostructured surfaces would appear as almost smooth for their anchoring elements, as can be observed in Figure 1b. On the contrary, staphylococci have dimensions of about 1 μm in diameter, and their cell walls are much more rigid than eukaryotic cells. In general, bacteria have a characteristic shape and are much less deformable. Due to their smaller size, bacteria are sensitive to the nanotopography and to the nanocolumns. In fact, as it was previously pointed out by Mitik-Dineva et al [42], our study shows that bacteria are susceptible to nanoscale surface roughness. Specifically, the high density of nanocolumns seems to force *S. aureus* to attach to Nano-Ti6Al4V samples through a limited number of anchoring points at the top of the nanocolumns (about 20 to 30 nanocolumns as can be estimated in Fig. 1c), thus reducing the area available for bacterial attachment. Together with the lotus leaf effect exhibited by these nanosurfaces, the adhesion of *S. aureus* is strongly impeded onto nano-Ti6Al4V. Although the chemical properties of biofilms may vary depending upon the microbial specie, the adhesion of bacteria (both specific and unspecific) is a mandatory stage in biofilm formation. In this sense, the physic-chemical interaction between surface and bacteria plays a fundamental role in the adhesion stage.[43] Our findings indicate that the nanocolumns prepared by MS-GLAD exert a very important influence on biofilm inhibition by acting on the unspecific stage of bacterial growth.

4. Conclusion

Titanium nanocolumnar coatings provide new perspectives for manufacturing Ti6Al4V-based implants for bone tissue repair, as they demonstrate the possibility of

manufacturing drug free surfaces that simultaneously exhibit opposite response to osteoblasts and *S. aureus*.

Acknowledgements

This study was supported by research grants from Ministerio de Ciencia e Innovación (MICINN) through the projects MAT2012-35556 and CSO2010-11384-E (Agening Network of Excellence), the Spanish MINECO (Projects CONSOLIDER CSD2008-00023, MAT2011-29194-C02-01, MAT2013-40852-R and MAT2013-43299-R) and the Junta de Andalucía (projects P12-FQM-2265 and P10-FQM-6900).)

References

[1] Arcos D, Boccaccini AR, Bohner M, Díez-Pérez A, Epple M, Gomez-Barrena E, et al. The relevance of biomaterials to the prevention and treatment of osteoporosis. Acta Biomater 2014;*10*:1793-805.

[2] Campoccia D, Montanaro L, Ariola CR. The significance of infection related to orthopedic devices and issues of antibiotic resistance. Biomaterials 2006;27:2331-39.

[3] Gioe TJ, Killeen KK, Grimm K, Mehle S, Scheltema K. Why are total knee replacements revised? Analysis of early revision in a community knee implant registry. Clin Orthop Relat Res. 2004;428:100-6.

[4] Fitzgeral RH. Prevention and diagnosis. Orthop Clin N Am 1992;23:259-64.

[5] Urban JA, Garvin KL. Prosthetic joint infection. Curr Treat Options Infect Dis. 2003;413:261-8.

[6] Foster TJ. The Staphylococcus aureus "superbug" J Clin Invest. 2004;114:1693-6.

[7] Harris LG, Richards RG. Staphylococcus aureus adhesion to different treated titanium surfaces. J Mater Sci: Mater Med. 2004;15: 311-4.

[8] Götz F. Staphylococcus and biofilms. Mol Microbiol 2002;43:1367-78.

[9] Konig C, Schwank S, Blaser J. Factors compromising antibiotic activity against biofilms of Staphylococcus epidermidis. Eur J Clin Microbiol Infect Dis. 2001;20:20-6.

[10] Stewart PS. Mechanisms of antibiotic resistance in bacterial biofilms. Int J Med Microbiol.2002;292:107-13.

[11] Campoccia D, Montanaro L, Arciola CR. A review of the biomaterials technologies for infection-resistant surfaces. Biomaterials. 2013;34:8533-54.

[12] Puckett SD, Taylor E, Raimondo T, Webster TJ. The relationship between the nanostructure of titanium surfaces and bacterial attachment. Biomaterials. 2010;31:706-13.

[13] Díaz C, Schilardi PL, Salvarezza RC, Fernández-Lorenzo M, Mele D. Nano/Microscale order affects the early stages of biofilm formation on metal surfaces. Langmuir 2007;23:11206-10.

[14] Jahed Z, Lin P,. Seo BB, Verma MS, Gu FX, Tsui TY, et al. Responses of Staphylococcus aureus bacterial cells to nanocrystalline nickel nanostructures. Biomaterials 2014;35:4249-54.

[15] Webster TJ, Ejiofor JU. Increased osteoblast adhesion on nanophase metals: Ti, Ti6Al4V, CoCrMo. Biomaterials. 2004;25:4731-9.

[16] de Oliveira PT, Zalzal SF, Beloti MM, Rosa AL, Nanci A. Enhancement of in vitro osteogenesis on titanium by chemically produced nanotopography. J Biomed Mater Res. 2007;80A;554-64.

[17] Webster TJ, Ergun C, Doremus RH, Siegel RW, Bizios R. Enhanced functions of osteoblasts on nanophase ceramics. Biomaterials. 2000;21:1803-10.

[18] Anselme K, Davidson P, Popa AM, Giazzon M, Ploux L, The interaction of cells and bacteria with surfaces structures at the nanometre scale. Acta Biomater. 2010;6:3824-46.

[19] Colon G, Ward BC, Webster TJ. Increased osteoblast and decreased Staphylococcus epidermidis funcitions on nanophase ZnO and TiO2. J Biomed Mater Res A 2006;78:595-604.

[20] Ploux L, Anselme K, Dirani A, Ponche A, Soppera O, Roucoules V. Opposite responses of cells and bacteria to micro/nanopatterned surfaces prepared by pulsed plasma polymerization and UV-irradiation. Langmuir 2009;25:8161-9.

[21] Mei S, Wang H, Wang W, Tong L, Pan H, Ruan C, et al. Antibacterial effects and biocompatibility of titanium surfaces with graded silver incorporation in titania nanotubes. Biomaterials. 2014;35:4255-65.

[22] Decuzzi P, Ferrari M. Modulating cellular adhesion through nanotopography. Biomaterials. 2010;31:173-9.

[23] Sengstock C, Lopian M, Motemani Y, Borgmann A, Khare C, Buenconsejo PJS, et al. Structure-related antibacterial activity of a titanium nanostructured surface fabricated by glancing angle sputter deposition. Nanotechnology 2014;25:195101.

[24] Alvarez R, García-Martín JM, Macías-Montero M, González-García L, González JC, Rico V, et al. Growth regimes of porous gold thin films deposited by magnetron sputtering at oblique incidence: from compact to columnar microstructures. Nanotechnology 2013;24:045604.

[25] Sit JC, Vick D, Robbie K, Brett MJ. Thin film microstructure control using glancing angle deposition by sputtering J Mater Res 1999;14:1197-9.

[26] Kelly PJ, Arnell RD. Magnetron sputtering: a review of recent developments and applications. Vacuum. 2000;56:159-172.

[27] García-Martín JM, Alvarez R, Romero-Gómez P, Cebollada A, Palmero A. Tilt angle control of nanocolumns grown by glancing angle sputtering at variable argon pressures.Appl Phys Lett 2010;97:173103.

[28] Terriza A, Díaz-Cuenca A, Yubero F, Barranco A, González-Elipe AR, González-Caballero JL, et al. Light induced hydrophilicity and osteoblast adhesion promotion on amorphous TiO_2.J. Biomed. Mater. Res. A 2013;101A:1026-35.

[29] Ivanova EP, Hasan J, Webb HK, Truong VK, Watson GS, Watson JA, et al. Natural Bactericidal Surfaces: Mechanical Rupture of Pseudomonas aeruginosa Cells by Cicada Wings.mall. 2012;8:2489-94.

[30] Guo Z, W. Liu, B.L. Su J.A. Superhydrophobic surfaces: From natural to biomimetic to functional. J Coll Interf Sci. 2011;353:335-55.

[31] Singh DP, Singh JP. Enhanced Evaporation of Sessile Water Droplet on Vertically Standing Ag Nanorods Film. J Phys Chem C. 2011;15:11914.

[32] Kumar DA, Xavier JA, Shya JM, Xavier FP. Synthesis and structural, optical and electrical properties of TiO_2/SiO_2 nanocomposites. J. Mater. Sci. 2013;48:3700-7.

[33] Dillon AC, Ott AW, Way JD, George SM. Surface chemistry of Al_2O_3 deposition using $Al(CH_3)_3$ and H_2O in a binary reaction sequence. Surf. Sci. 1995;322:23042.

[34] Arenas MA, Perez-Jorge C, Conde A, Matykina E, Hernandez-Lopez JM, Perez-Tanoira de Damborenea JJ, et al. Doped TiO_2 anodic layers of enhanced antibacterial properties. Colloids Surf. B Biointerfaces. 2013;105:106-12.

[35] Ross AM, Jiang Z, Bastmeyer M, Lahann J. Physical Aspects of Cell Culture Substrates: Topography, Roughness, and Elasticity. Small 2012;8:336-355.

[36] Anselme K. Osteoblast adhesion on biomaterials. Biomaterials 2000;21:667-81.

[37] Hunter A, Archer CW, Walker PS, Blunn GW. Attachment and proliferation of osteoblasts and fibroblasts on biomaterials for orthopaedic use. Biomaterials. 1995;16:287-95.

[38] Links J, Boyan BD, Blanchard CR, Lohmann CH, Liu Y, Cochran DL, et al. Response of MG63 osteoblast-like cells to titanium and titanium alloy is dependent on surface roughness and composition. Biomaterials. 1998;19:2219-32.

[39] Fuita S, Ohshia M, Iwaa H. Time-lapse observation of cell alignment on nanogrooved patterns. J R Soc Interface. 2009;6:S269-77.

[40] Texeira AI, Abrams GA, Bertics PJ, Murphy CJ, Nealey PF. Epithelial contact guidance on well-defined micro- and nanostructured substrates. J Cell Sci. 2003;116:1881-92.

[41] Loesberg WA, Riet J, van Delft FCMJM, Schön P, Figdor CG, Speller S. The threshold at which substrate nanogroove dimensions may influence fibroblast alignment and adhesion. Biomaterials 2007;22:3944-51.

[42] Mitik-Dineva N, Wang J, Mocanasu RC, Stoddart PR, Crawford RJ, Ivanova EP. Impact of nano-topograpy on bacterial attachment. Biotechnol J. 2008;3:536-44.

[43] Ploux L, Ponche A, Anselme K. Bacteria/material interfaces: role of the material and cell Wall properties. J Adhesion Sci Technol. 2010;24:2165-201.

Figure captions

Fig. 1. SEM micrographs of (a) Ti6Al4V substrate; (b) Nano-Ti6Al4V sample; selected area indicates an estimation of an osteoblast size; (c) Nano-Ti6Al4V; selected area indicates an estimation of a *S. aureus* size; (d) SEM image of a Nano-Ti6Al4V cross section showing the nanocolumns. Evaluation of surface wettability; (e) micrograph of a water drop onto a Ti6Al4V substrate. (f) micrograph of a water drop onto a Nano-Ti6Al4V sample.

Fig. 2. XRD patterns of Nano-Ti6Al4V (up) and Ti6Al4V (down) samples collected with gracing incidence angle (Ω= 0.5º). Miller indexes are indicated for the TiO_2 rutile phase. Stars (*) indicate diffraction maxima corresponding to α-Ti .

Fig. 3: FTIR spectra of Nano-Ti6Al4V (down) and Ti6Al4V (up) samples collected by Attenuated Total Reflectance (ATR).

Fig. 4: AFM images of Ti6Al4V (a) and Nano-Ti6Al4V (b), the color scale for the height being Zmax=46 nm and Zmax=380 nm for Ti6Al4V and Nano-Ti6Al4V, respectively

Fig. 5. Osteoblast adhesion after 90 minutes onto a Ti6Al4V substrate and a Nano-Ti6Al4V sample (a). Mitocondrial activity (MTT test) after 3 days of osteoblast culture onto Ti6Al4V and Nano-Ti6Al4V (b). SEM micrographs obtained after 24 hours of culture with osteoblast cells onto Ti6Al4V substrate (c) and (d); and Nano-Ti6Al4V sample (e) and (f). Non statistically significant ($p < 0.05$) differences were observed in osteoblast adhesion (a) neither in MTT tests (b).

Fig. 6. Bacterial adhesion tests carried out by inoculation of *S. aureus* 15981collection strain and several clinical strains onto Ti6Al4V and Nano-Ti6Al4V surfaces.(* significant differences $p<0.001$, Kruskal -Wallis test).

Fig. 7. SEM micrographs of samples Ti6Al4V (left) and Nano-Ti6Al4V (right) after 24 hours of culture with *S. aureus*. The micrographs show a biofilm formation onto Ti6Al4V, whereas nano-roughness is still visible onto Nano-Ti6Al4V. In the Ti6Al4V, bacteria covered by the extracellular matrix (arrow), which is an essential part of a biofilm, are observed. In the Nano-

Ti6Al4V sample, only bacterial cells without production of extracellular matrix are observed (arrow).

Fig. 8. (a) Images collected by confocal fluorescence microscopy after 1.5, 6 and 24 hours of culture with *S. aureus* onto Ti6Al4V and Nano-Ti6Al4V surfaces. Ti6Al4V shows initial bacterial adherence (1.5 hours, arrow), and subsequent development of biofilm (6 and 24 hours, arrows). Biofilms can be seen as bacterial conglomerates embedded in the extracellular matrix (arrows). No biofilms are observed in the modified material Nano-Ti6Al4V, and only cells and small conglomerates can be seen (arrows); **(b)** confocal 3D reconstruction of Ti6Al4V surface after 24 hours of culture. Both extracellular matrix and bacteria are observed. **(c)** Confocal 3D reconstruction of Nano-Ti6Al4V surface after 24 hours of culture. Only alive individual bacterial cells can be detected without biofilm formation.

Figure 1

Click here to download high resolution image

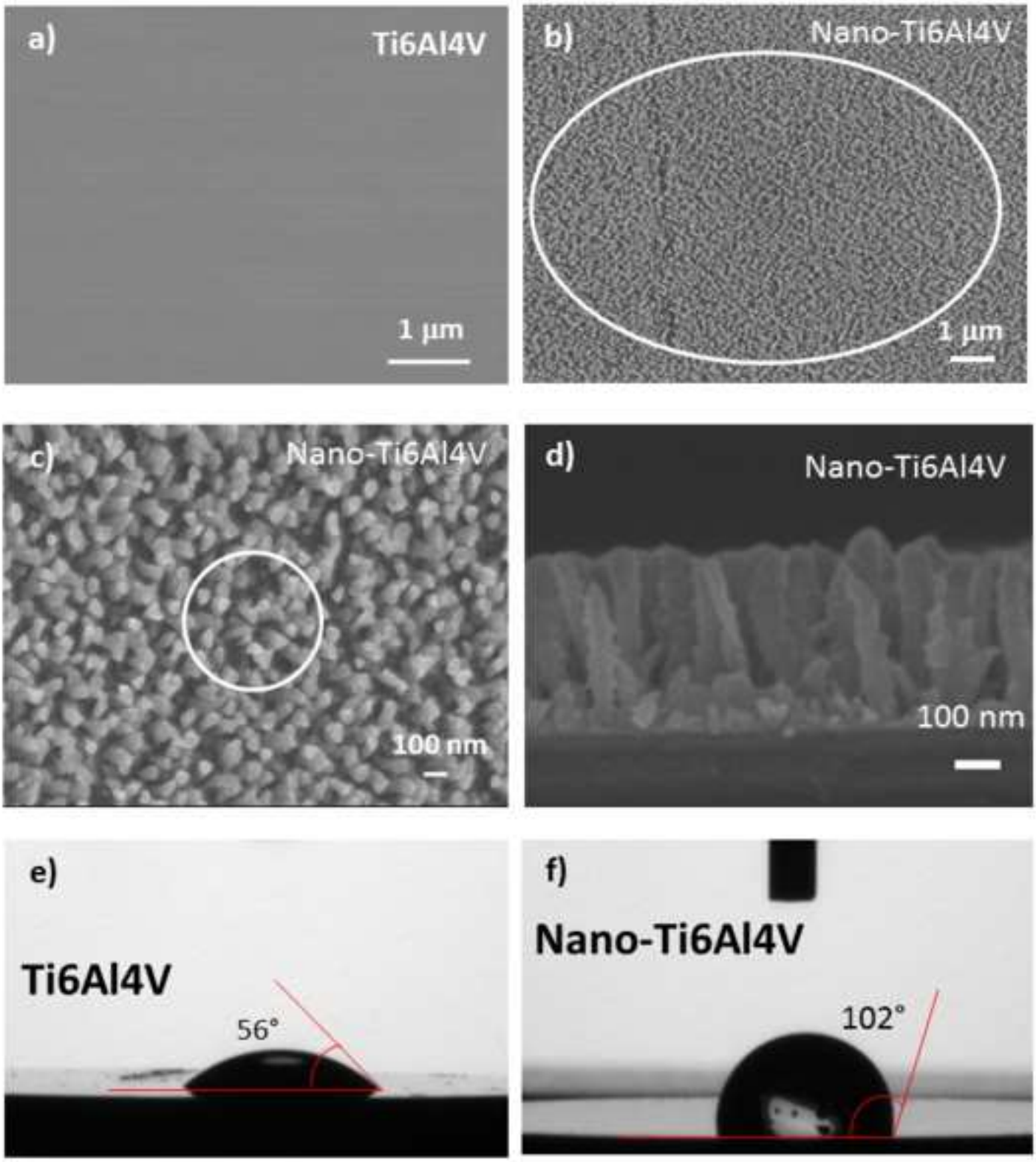

Figure 2

Click here to download high resolution image

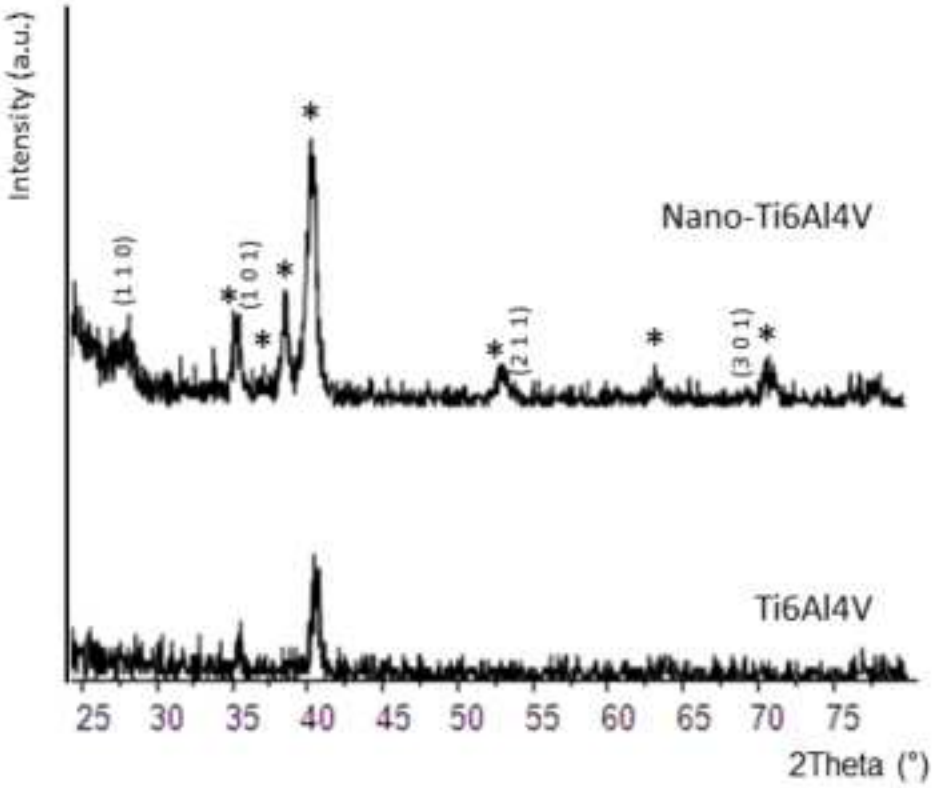

Figure 3

Click here to download high resolution image

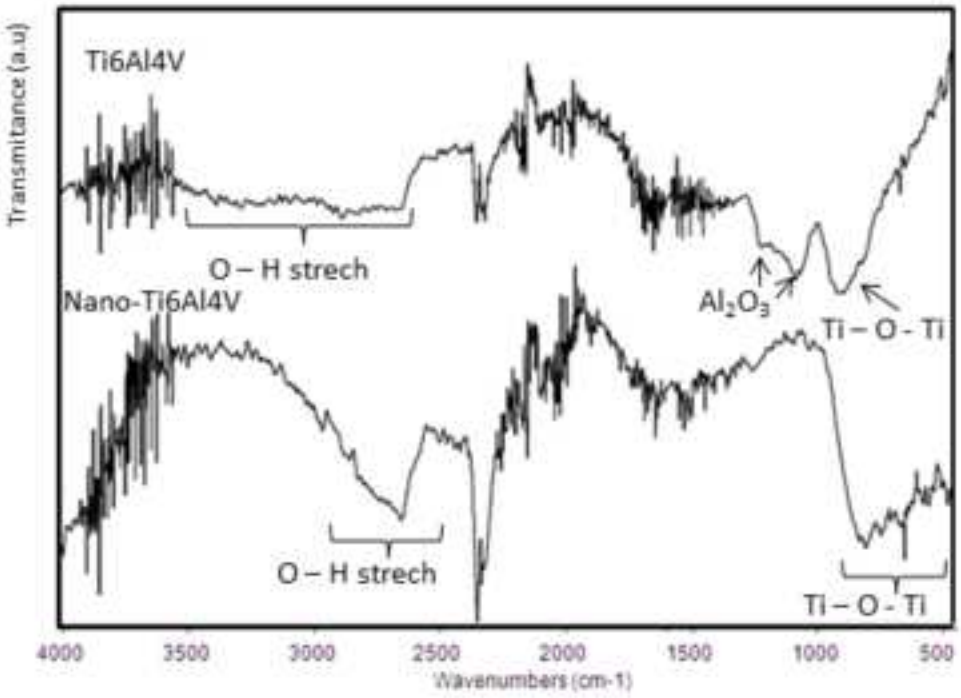

Figure 4

Click here to download high resolution image

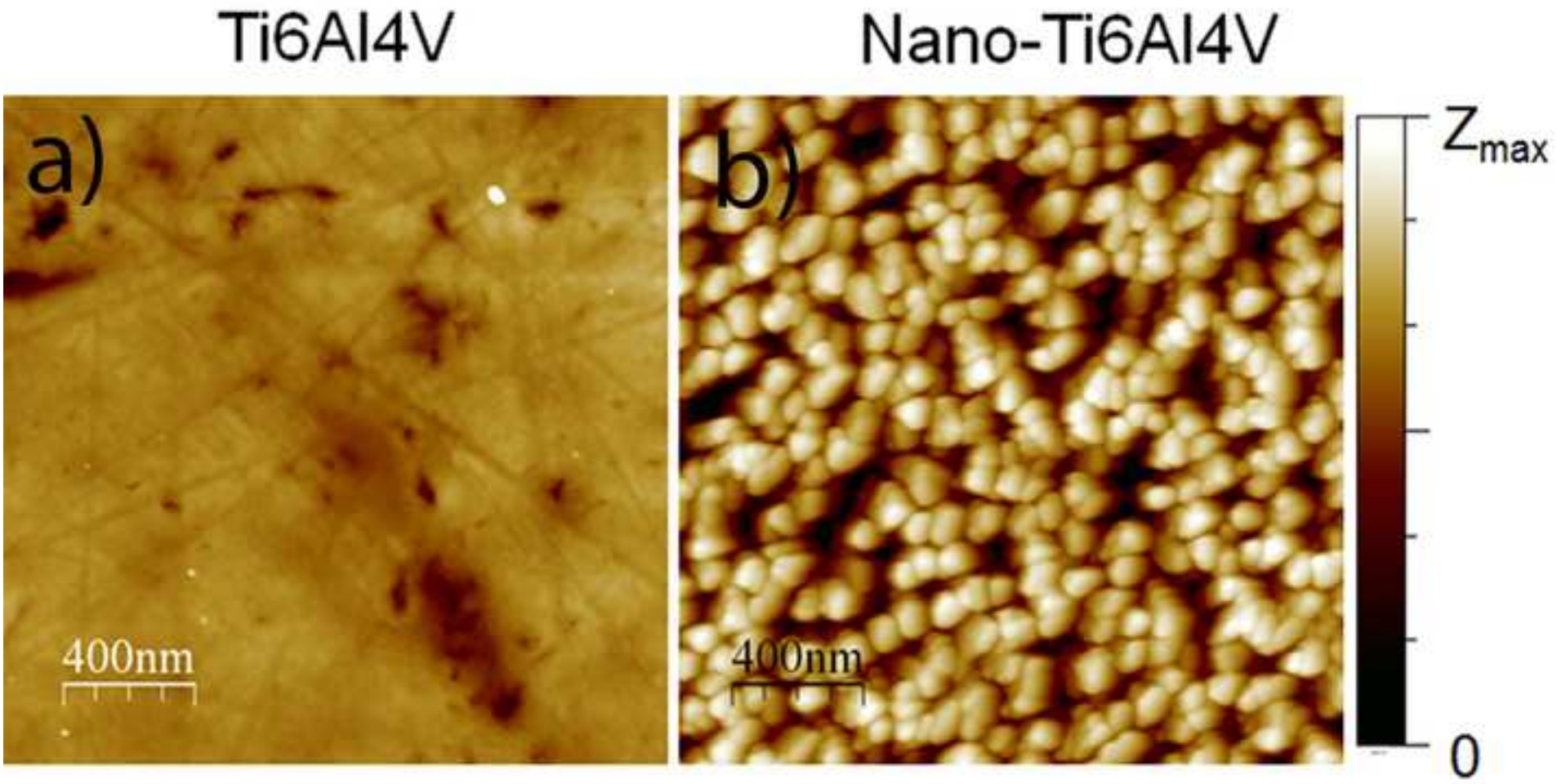

Figure 5

Click here to download high resolution image

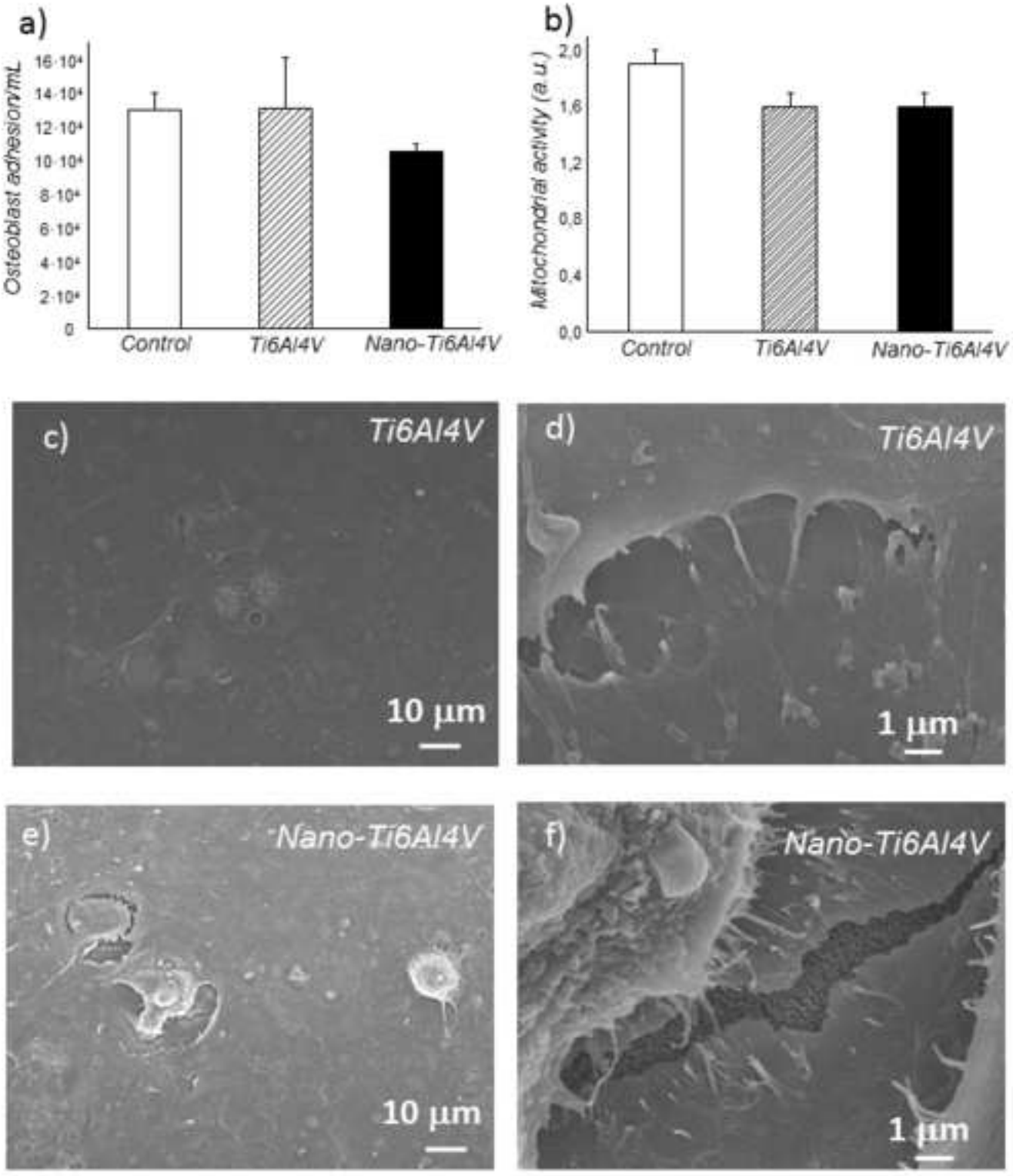

Figure 6

Click here to download high resolution image

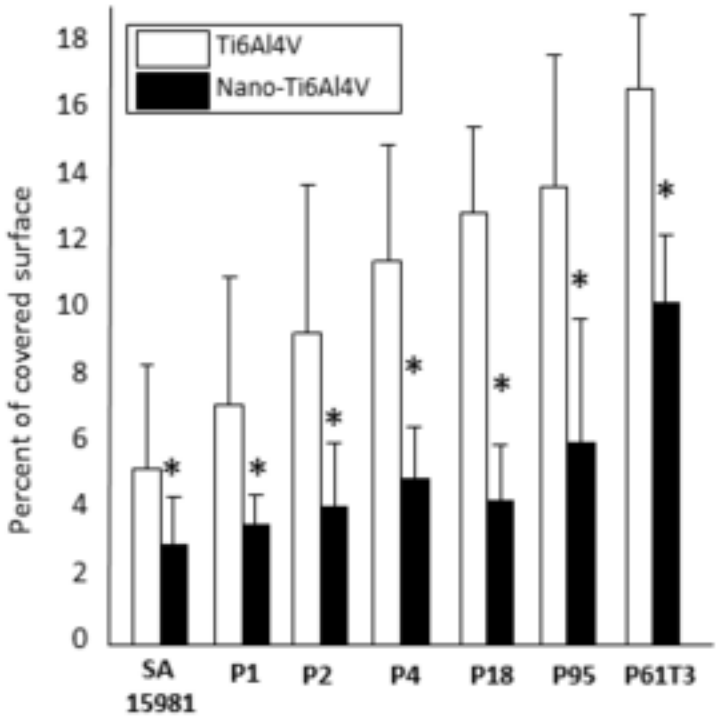

Figure 7

Click here to download high resolution image

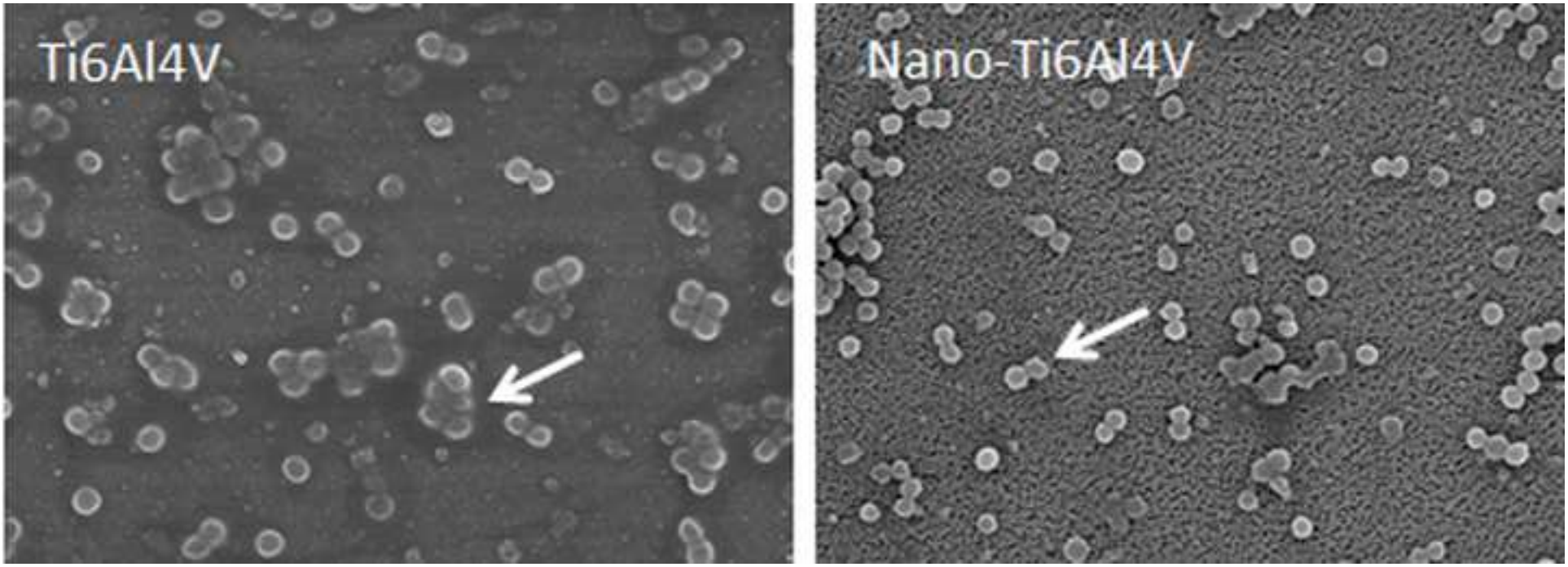

Figure 8

Click here to download high resolution image